

---

# Positron Emission Mammography

---

Mónica Vieira Martins

Additional information is available at the end of the chapter

<http://dx.doi.org/10.5772/60452>

---

## 1. Introduction

### 1.1. Motivation

Breast cancer imaging is a good example of how medical imaging modalities can diminish the number of patients suffering from this highly prevalent and deadly disease. X-ray mammography is the most used technique for breast cancer imaging. This technique is used either as a complementary tool to clinical diagnosis or as an irreplaceable screening tool for the early detection of the disease. However, it suffers from low specificity in the detection of malignancy and low sensitivity in women with dense breast tissue. Other imaging methods such as breast Ecography and breast Magnetic Resonance Imaging play important roles as adjunct techniques to X-ray mammography. The information provided by the aforementioned techniques is, however, mainly anatomical, thus leaving space for imaging methods that are able to obtain information regarding functional or metabolic changes in tissues.

Among these, molecular imaging methods using labeled radiotracers such as Scintigraphy, SPECT, Positron Emission Tomography (PET) and PET-CT, have been found to provide useful complementary information to the anatomical methods regarding detection, diagnosis and staging of breast cancer. However, the standard technology of whole body scanners, due to its limited spatial resolution, and to its disadvantageous geometry, which limits sensitivity, have in part precluded molecular imaging using radiotracers from contributing with its full potential to the imaging of the breast.

These limitations have prompted an active interest in the development of compact positron emission tomography cameras dedicated for breast imaging, a technique named Positron Emission Mammography. In the last 20 years there has been a tremendous effort from the industry and the scientific community to develop such devices, with a variety of detector designs and geometries, innovative radiation detection schemes, new scintillation crystals and adapted image reconstruction algorithms being studied in order to optimize the technique.

Either as prototypes or as commercial equipment, PEM scanners have provided data that confirms a huge improvement in technical characteristics with regards to whole body scanner, thus showing great promise of becoming a valuable modality in the clinical practice. In fact, Positron Emission Mammography, for which there are now two commercial equipment available, has demonstrated higher detectability than PET/CT and comparable or better sensitivity than MRI. It seems now to be clear that PEM is a valuable technique when MRI cannot be used.

In this chapter we will present a review from the literature of the main equipment that have been developed for Positron Emission Mammography, emphasizing the different approaches that have been followed in the design of the scanners, the main technical outcomes and, when such information is available, the most significant results obtained in the clinical trials.

The chapter will begin with a brief description of the principles behind the tomographic method for molecular imaging of positron emission isotopes. We will then review the performance parameters and instrumentation issues more challenging in the design of dedicated PEM scanners. We will review the PEM clinical results available so far, which allow a direct comparison between PEM, PET and MRI, and which give some clues regarding the clinical utility of PEM.

## **2. Positron emission mammography technology**

The principles underlying Positron Emission Mammography are similar to those of Positron Emission Tomography. However, since there is a requirement for high resolution and high sensitivity, specific instrumentation issues are raised during the design and development of PEM scanners. This section will begin by presenting the principles of positron emission detection for medical imaging purposes; then, the key factors regarding the technical performance of the scanner will be presented. A very brief overview on the most important issues regarding the image reconstruction will also be presented.

### **2.1. Positron emission and detection**

Positron Emission Mammography, as well as Positron Emission Tomography, uses radiopharmaceuticals that are labeled with a positron emitting radionuclide.

The most used radiopharmaceutical for imaging cancer in PET is 18F-fluorodeoxyglucose, or  $^{18}\text{F}$ -FDG, a glucose analogue that is labeled with the positron emitter  $^{18}\text{F}$ . This radiotracer is used to detect glucose consumption, which is known to be increased in cancerous cells compared to normal cells. This is due to the higher metabolism of cancerous cells. The advantage of being able to image metabolism instead of anatomy, like in CT, is that the accelerated metabolic activity of cancerous cells occurs before the changes in the anatomical structures are detectable.

The tracking mechanism of 18FDG inside the cancerous cells is as follows. FDG is a glucose analog and, just like glucose, is transported into the cells by glucose transporters named

GLUT1. These transporters are known to be overexpressed in breast cancerous cells, thus contributing to increased FDG uptake [1]. Once inside the cell, FDG is phosphorylated into deoxyglucose-6-phosphate (FDG-6-PO<sub>4</sub>) by an enzyme named hexokinase. Hexokinase is also thought to be overexpressed in cancerous cells. Unlike glucose, FDG-6-PO<sub>4</sub> does not enter further enzymatic reactions and, due to its negative charge, it remains trapped inside the cell [2]. This metabolic trapping of FDG inside the cell constitutes the basis for imaging the *in vivo* distribution of the tracer.

Besides <sup>18</sup>F, other radionuclides, such as <sup>82</sup>Rb, <sup>15</sup>O, <sup>13</sup>N and <sup>11</sup>C, among others, can be used to label the molecular probes used in PET.

Once emitted from the radiopharmaceutical, the positron travels a given amount of space in matter, while dissipating its kinetic energy through interactions with electrons and surrounding nuclei. At the end of its path, the positron combines with an electron in its vicinity, in an annihilation reaction whereby the total mass of the electron and the positron is converted into high energy photons. The rest-mass energy of both positron and electron is 511 keV. If both particles are at rest at the time of annihilation, the two resulting 511 keV photons will be emitted in opposite directions.

The gamma rays thus emitted can interact with the tissues of the patient either by photoelectric effect or by Compton scatter. Both photon attenuation and scatter result in image degradation since, in the first case, emission counts are lost and, in the second, the measured spatial information is inaccurate. Whereas the correction for the effect of attenuation is fairly simple if a transmission scan is available, the correction for the scatter effect not as straightforward.

If the photons are not absorbed by the matter in the patient body, they can be detected externally in coincidence by using opposed pairs of scintillator crystals. Each luminous signal produced in the crystals is transformed into an electrical signal. A coincidence event happens when such two electrical signals are registered in a coincidence electronic circuit within a time frame that is defined by a coincidence time window.

The imaginary line that unites the two activated crystals in a coincidence event is called a line of response (LOR). The number of counts that are detected along the several LORs during an exam is stored in an histogram and used for image reconstruction purposes. Alternatively, list mode format can be used. In list mode format, the relevant information regarding the event, such as the activated crystals, the deposited energy and a time stamp, is stored sequentially on disk and used directly for image reconstruction.

## 2.2. The performance of a scanner

Of main importance for the performance of a PET scanner are its photon sensitivity and its spatial, energy and temporal resolutions. The geometry, the detector crystals and the electronics of the system all impact on the above. In this paragraph we will overview the main aspects that affect these parameters, highlighting the most common differences between traditional clinical scanners and high resolution scanners.

The **photon sensitivity** is defined as the fraction of 511 keV photon pairs emitted from the imaging subject that are detected by the imaging system [3]. It is important that a scanner has

the higher photon sensitivity possible since a higher fraction of detected photons will impact on better statistics of the acquired data and, consequently, on lower noise level of the final reconstructed images. The photon sensitivity in a clinical PET system is low. In dedicated or high resolution scanners, The sensitivity is usually improved by increasing the scanner geometric efficiency, that is, the probability that the emitted photon transverses the detected material, or by increasing the intrinsic detector efficiency.

Usually, the scanner geometric efficiency is enhanced in dedicated scanners relatively to traditional scanners mainly because the detector is brought closer to the imaging subject.

The geometric efficiency can also be increased by packing the detector elements as tightly as possible and by covering the region to be imaged with as much detector as possible. The other aspect that influences the scanner photon sensitivity is the intrinsic detector efficiency. This is defined as the likelihood that photons transversing the detector material will be stopped [3]. It depends mainly on the scintillator crystals that are used as detector elements. Scintillator crystals that have high density ( $\rho$ ), with high effective atomic number ( $Z_{\text{eff}}$ ) have maximum ability to stop the 511 keV photons. In fact, a high density crystal favors the photon interaction and a high effective atomic number maximizes the probability of photoelectric interactions within the crystal, with respect to Compton events. The quantity that maximizes the crystal stopping power is  $\rho \cdot Z_{\text{eff}}^5$ . A scintillator that has a high stopping power will have a short attenuation length.

Table 1 lists the values of  $Z_{\text{eff}}$ ,  $\rho$ , the attenuation length and some other properties of the most common scintillator crystals used in PET scanners. The decay time determines the time resolution of the scanner and the light output determines the detector energy resolution and has effects also in the image resolution. Both these parameters will be discussed later.

Sodium iodide doped with thallium (NaI(Tl)) was the detector initially used in PET scanners. It has a very high light output (38 photons/keV), resulting in good energy and spatial resolutions [4]. However, its slow decay time leads to increased detector dead time and a high random coincidence rate (see below the discussion for system time resolution). Its low density results in a low stopping power (high attenuation length) when compared to the other crystals used in PET. Sodium iodine was first replaced by BGO (bismuth germanate:  $\text{Bi}_4\text{Ge}_3\text{O}_{12}$ ) that, despite its high decay time and poor light output, has an excellent stopping power.

More recently, other crystals that combine better light output with high stopping power have been introduced to PET. LSO (lutetium oxyorthosilicate:  $\text{Lu}_2\text{SiO}_5$ ) has a high stopping power and a good light yield but, due to intrinsic properties of the crystal, its overall resolution is not as good as NaI(Tl) [5]. GSO (gadolinium orthosilicate:  $\text{Gd}_2\text{SiO}_5$ ), despite its lower stopping power and light output, has better energy resolution than LSO. Both crystals are in use in PET scanners.

The **spatial resolution** describes the ability of the system to distinguish two closely spaced point sources. In PET, the fundamental limit of spatial resolution is imposed by the nature of positron annihilation. In fact, the emitted positron describes, before annihilating, a given path of variable length and direction. Therefore, the detected LOR contains the positron annihilation

	Effective Z	Density (g/cm <sup>3</sup> )	Attenuation length (mm)	Relative light output (% NaI)	Decay time (ns)
Sodium Iodide	51	3.7	29.1	100	230
BGO	75	7.2	10.4	15	300
LSO	66	7.4	11.4	75	42
GSO	59	6.7	14.1	20	60
LYSO	65	7.1	1.2	107	40
LuAP	65	8.3	*	30	17
LuYAP	60	7.1	*	34	23

**Table 1.** Properties of common scintillator crystals used in positron emission tomography. Adapted from [3] and from [6] (LuAP and LuYAP data). \* Data not found.

point, not the positron emission point, and these two points can be several millimeters apart. This positron range effect degrades the spatial resolution of the images. (Figure 1a). The positron range depends upon the energy of the emitted positron and upon the electronic density of the medium. It has been estimated a value of 0.22 mm FWHM for the positron range emitted from <sup>18</sup>F in water, the major component of human cells [7].

In addition to the positron range, the acollinearity effect also leads to resolution degradation in PET systems. This effect is caused by the fact that the annihilation photons are almost never anti-parallel, since usually the positron and the electron are not exactly at rest when they annihilate. As a consequence, the detected line of response does not contain the point of positron-electron annihilation (Figure 1b). The degradation of the spatial resolution due to the acollinearity effect worsens as the detector diameter increases.

Another significant factor that limits PET spatial resolution is the size of the detector element. Spatial resolution may be improved significantly by reducing the detector pixel size. This is especially important in small diameter or dedicated PET scanners, where the pixel size dominates image resolution over the non-collinearity effect, which is minor for small detector diameters. Typical clinical systems use 4.0–6.0 mm detector pixel sizes, whereas small animal use detector pixels of 1.5–2.0 mm and positron emission mammography scanners use pixel sizes of 1.8–3.0 mm.

A final important factor that affects PET spatial resolution is the parallax error. This error occurs when the crystal depth at which the photon interaction takes place, known as Depth of Interaction (DOI), is not known. In this case, the LOR that unites the two activated crystals does not necessarily contain the true LOR (Figure 1c). For photons entering the scintillators at oblique angles there will be a mismatch between the true and the measured line of response. This degrading effect has greater impact in scanners where the distance between opposed detectors is smaller, like dedicated cameras. Good spatial resolution is of crucial importance for these cameras.

To improve photon sensitivity, the scintillator crystals that compose these dedicated scanners are usually long crystals. Therefore, not surprisingly, the ability to obtain DOI information has become an important factor in the design of high resolution PET scanners [8], with different strategies being followed to perform such measurements.

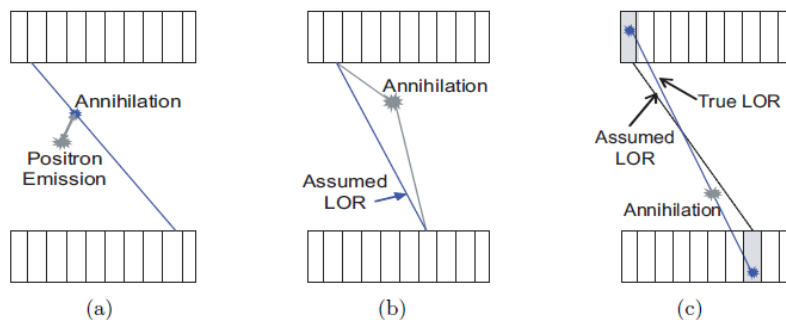


**Figure 1.** Schematic drawings of some of the effects that degrade spatial resolution in PET: a) the positron range, b) the accolinearity effect and c) the Depth of Interaction effect or parallax error.

The **energy resolution** indicates the precision with which the system can measure the incoming photon energy. A good energy resolution is important because it allows the use of a narrow energy window without significantly compromising photon sensitivity.

A narrow energy window helps to prevent contamination from photons that undergo scatter before interacting with the scintillator crystal, since the scatter process implies the loss of energy. It may also help to reduce the rate of random photon events, since a part of these photons undergo scatter. Random, or accidental, coincidences, occur when photons proceeding from different annihilations are detected within a same timing window and, although spatially uncorrelated, its detection is considered as a valid coincidence.

Energy resolution may be improved by using crystals with high scintillation light output. A typical value for clinical PET scanners energy resolution is 25% FWHM at 511 keV [3].

The **time resolution** determines how well the system can decide whether two incoming photons arrived simultaneously. Good time resolution allows the use of a narrow time window, thus reducing random event's detection without compromising photon sensitivity. The reducing of random events is also important as it helps to prevent the system from saturating in high count statistics studies. The parameter that most strongly determines the temporal coincidence timing window is the scintillator decay time: a fast scintillator allows the selection of a narrow time window. A typical value for clinical PET scanners time resolution is 3 ns FWHM at 511 keV [3].

The scintillation light from the crystals is read from **photodetectors**. In PET, are most commonly either photomultiplier tubes (PMT) or semiconductor based photodiodes. Photomultiplier tubes are the oldest and most reliable technology to detect and measure low levels of scintillation light. They have a high gain in the photoelectric conversion, which leads to high

signal-to-noise ratios. Besides simple PMT's, a class of PMTs has been developed that provides not only energy information but also spatial information about the detected light. These PMTs, named Position-Sensitive PMTs (PS-PMT) have been found to be useful in the design of high resolution PET scanners [9].

PMTs have two major drawbacks. They have low quantum efficiency, meaning that the ratio between the incident photons and the primary produced electrons is low. In addition, PMTs are big devices, often with a small field of view, and this may constitute a drawback, especially when they are to be used in small dedicated scanners. In recent years there has also been great progress in the development of semiconductor photodetector arrays. These can be the PIN photodiode, the avalanche photodiode (APD) and the silicon drift detector (SDD). Among these, the APDs are the most used in PET cameras. Semiconductor photodetectors have many advantages over PMTs: they are very compact; they are insensitive to magnetic fields, which makes them good candidates for PET-MRI devices; they are available with large active areas; they have a very high efficiency [10]. The main disadvantages of APDs are their sensitivity to temperature and bias voltage.

### 2.3. Image reconstruction

For many years, the problem of reconstructing an image from the projection data acquired in Positron Emission Tomography was addressed with analytic approaches which were inherited from X-ray computed tomography. Analytic algorithms such as filtered backprojection (FBP) are based on the direct inversion of the Radon transform. They are fast, linear, predictable, and their properties are very well known. The inversion of the Radon transform is derived for a continuous sampling and discretized afterward for sampled data [99]. Analytic algorithms are based on an idealized mathematical model for the data, the linear integral model, according to which the number of coincidence photon pairs detected along a LOR is approximately linearly proportional to the integral of the tracer density along a LOR. This model oversimplifies the physics inherent to the emission and detection processes in PET, limiting the accuracy of the images reconstructed with analytical algorithms.

In alternative to the analytic image reconstruction algorithms, model based algorithms, which can include accurate physical and statistical models of the systems, can be used. In opposition to analytical algorithms, they incorporate the discreteness of the data from the beginning. Their use usually results in improved image accuracy. As their formulation results frequently in large sets of nonlinear equations that must be solved by iterative methods, this class of algorithms is usually referred to as iterative image reconstruction algorithms. Furthermore, if statistical functions are used to derive them, they are said to be statistical iterative reconstruction algorithms. The use of iterative methods based on probability models for image reconstruction was already effective in the field of astronomy in the early 1970's (Lucy, 1974, Richardson 1972). Later, in 1976, Rockmore and Macovsky introduced the Maximum Likelihood approach in the field of medical imaging. The Ordered Subsets – Expectation Maximization (OSEM) algorithm was proposed in 1994 by Hudson and Larkin as an accelerated version of the ML-EM method and has since gained wide acceptance as a standard reconstruction method in PET. Nowadays, the most used algorithms for image reconstruction in PET belong to the class of iterative statistical algorithms.



### 3. Positron emission mammography scanners

A design of a dedicated positron emission imaging system for breast cancer was first presented in 1994 as a feasibility study for a positron emission mammography unit. Since then, more than ten other systems have been developed, two of which have become commercially available [11, 12]. Those systems differ in the number, geometry and mobility of the detectors used, with consequences on the patient positioning; its ability or not to perform biopsy; the different radiation detection scheme used, including different scintillation crystals; on the strategies used for image reconstruction from the measured projections. In this section we will review the instrumentation issues that impact on the performance of the equipment that use positron emission mammography to image disease. We will emphasize on the most demanding aspects of these dedicated instruments, showing why they hold the promise for an improved early detection of disease.

#### 3.1. The PEM-I system

A design of a dedicated positron emission imaging system for breast cancer was first presented in 1994 by Thompson [13] from the Montreal Neurological Institute of the McGill University, Canada, as a feasibility study for a positron emission mammography unit.

The developed scanner was designed to fit a mammographic unit, so that conventional mammograms could also be performed in the same gantry, thus allowing exact registration of the emission and of the conventional mammographic images [14]. For such purposes, the system included a co-registration tool to facilitate registration between radiographic and metabolic images [15]. A schematic diagram of the scanner is presented in Figure 2.

The developed scanner consists on two planar 2x2 detector arrays of blocks of bismuth germanate (BGO) crystals placed above and below the compressed breast. The detector blocks measure  $36 \times 36 \times 20 \text{ mm}^3$  and are segmented into  $1.9 \times 1.9 \text{ mm}^2$  pixels [16]. The separation between the detector heads can be adjusted to match the thickness of the breast. The system uses position sensitive photomultiplier tubes (PS-PMT) that are optically coupled to the crystal blocks. Although the PS-PMTs cover a surface of  $72 \times 72 \text{ mm}^2$ , their useful field-of-view (FOV) is only of  $65 \times 55 \text{ mm}^2$ . The coordinates of the coincidence on opposing PS-PMT faces are decoded by the system electronics and corrected for spatial distortion and efficiency [17].

The images from this system are obtained by performing a limited-angle weighted-backprojection algorithm. This consists on dividing the image into several equidistant planes and backprojecting the lines or response (LOR) onto those planes. With this technique, the image plane closest to the site of the tumor has the most focused image, while all the other planes present more blurred images, as it can be seen in the schematic diagram of Figure 3. This is known as the focal plane effect. The reconstruction scheme is said to be 'weighted backprojection' because the values that are added to a given plane in the image matrix are weighted accordingly to the probability of detection of an annihilation in that plane, the crystals efficiencies and the photon attenuation along the path to the crystal [14].



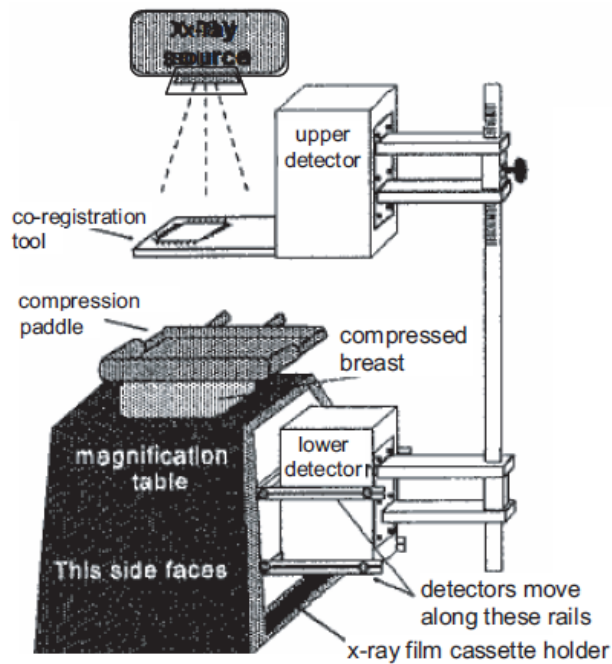


**Figure 2.** Schematic drawing of the PEM-I detector plates (white areas) mounted on a conventional mammographic unit (gray areas). From [15].

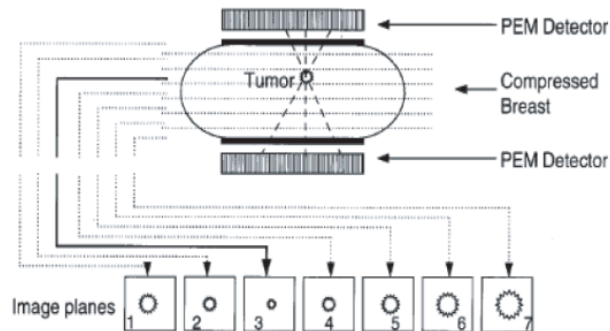


**Figure 3.** Weighted backprojection used in the PEM-I scanner. From [18].

The complete system has a spatial resolution of 2.8 mm FWHM, a time resolution of 12 ns and an efficiency of 3% at a detector separation of 55 mm [19]. It is estimated that the system is not able to detect tumors with a tumor-to-background ratio lower than 6:1 [20].

The preliminary clinical trials, performed with 16 subjects, reported 80% sensitivity and 100% specificity. The accuracy of the exam, computed as the ratio of the sum of the true findings (positive and negative) to the total number of lesions, was 86% [18]. For mammography exams performed on the same subjects, those values were, respectively, 90%, 50% and 81%. The smallest cancerous lesion detected with PEM-I was  $1.1 \times 1.1 \times 0.9 \text{ cm}^3$ . The lower value of sensitivity with PEM, with respect to mammography, was due, according to the authors, to the small FOV of the PEM device and to the impossibility of imaging tumors localized close to the chest wall (less than 2 cm). These limitations are related to the PMTs used, whose useful field of view is significantly smaller than its area, preventing imaging near their edges. Figure 4 shows a typical set of images obtained with PEM-I, each image corresponding to a plane of the sample, with a visible site of FDG uptake in a region close to the chest wall [19].



**Figure 4.** A typical set of images obtained with the PEM-I scanner. Each image corresponds to a plane, with the left-most image corresponding to the image plane closer to the upper detector. A visible site of FDG uptake can be seen in a region close to the chest wall. From [19].

### 3.2. The Naviscan PEM system

The original idea of Thompson for a PEM system was further developed by Weinberg and colleagues, for the Naviscan PET System. The Naviscan PEM Flex consists of two  $5.6 \times 17.3 \text{ cm}^2$  opposed detector heads [21] that can be fit on a stereotactic mammography unit [22]. This way, emission and transmission scans can be obtained. Data acquisition is performed by moving the detectors along a linear path, in order to image as much breast as possible. The PEM detectors translation allows to image an area equal to the entire X-ray field of view [23]. The system can also work separately from the mammography unit, allowing closer chest wall access. Figure 5 shows the PEM Flex system mounted in a stereotactic X-ray mammography unit.

Each detector head contains twelve  $13 \times 13$  crystal blocks, each coupled to a compact PS-PMT. The crystals are  $2 \times 2 \times 10 \text{ mm}^3$  of a mixed-lutetium silicate [21].

For each segment of the scan, list mode data are acquired, histogrammed and reconstructed by backprojection. This allows the operator to view partial images during the scan acquisition. At the end of the entire scan, the complete list mode data are reconstructed using a maximum-likelihood expectation-maximization algorithm.

The intrinsic spatial resolution of the system is 1.5 mm FWHM [23]. The image resolution is 2.5 mm FWHM in the plane perpendicular to the displacement and 6 mm between planes. Energy resolution was measured as 14% for 511 keV. The timing window used was 9 ns.

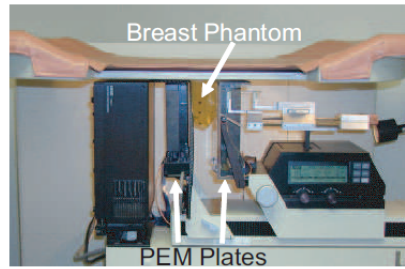


**Figure 5.** The PEM Flex system mounted in a stereotactic X-ray mammography unit. From [22].

The clinical trials performed so far [24, 25] were all performed on patients with known breast cancer or suspected lesions. Hence, they provide little information on the specificity of the technique. In one of these studies [25], PEM was able to visualize 39 out of 44 lesions. The non visualized lesions ranged in size from a 1 mm ductal carcinoma in situ (DCIS) to a 1 cm infiltrating ductal carcinoma. Some lesions could not be visualized due to limitations on how posterior the breast tissue is observable by the device. Others, as interpreted by the authors of the study, due to the variability in the metabolic activity of breast cancer cells, similarly to what happens with whole body PET.

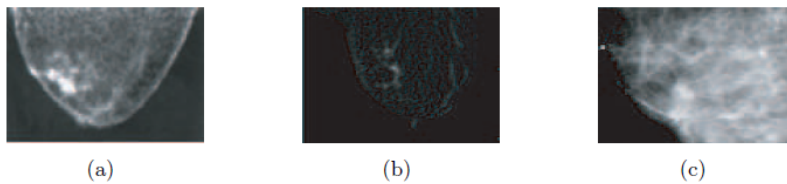


**Figure 6.** Image of DCIS obtained with the PEM Flex scanner a), with MRI b) and with mammography c). Neither MRI nor mammography could detect the DCIS lesion seen in the PEM image. From [25].

The most encouraging finding in this trial was the fact that PEM was able to visualize DCIS not visualized by mammography, breast ecography or MRI. An example of such a case can be seen in Figure 6. The smallest lesion detected by PEM in this study was a 2 mm duct of DCIS. This preliminary clinical trial seems to indicate that the technology is promising and worthy of further investigation.

### 3.3. The West Virginia University — Jefferson Lab PEM system

Another PEM system was developed and tested at the West Virginia University and at the Jefferson Laboratory by Raylman and colleagues [26]. This PEM system, which is mounted on a stereotactic biopsy table, consists of two square  $10 \times 10 \text{ cm}^2$  detector arrays of discrete  $3 \times 3 \times 10 \text{ mm}^3$  GSO crystals. The scintillation light is collected by arrays of PS-PMTs. An image of the scanner mounted on the biopsy table, together with a torso phantom can be seen in Figure 7.



**Figure 7.** Image of the West Virginia University - Jefferson Laboratory PEM system. The PEM detector heads, mounted in a biopsy table, are highlighted by the black arrows. A torso phantom can be seen in the table. From [27].

Since one of the goals of the system is to perform PEM guided biopsies, a trigonometric algorithm was developed to determine the lesion stereotactic coordinates. This algorithm uses two PEM images that are acquired at two symmetric angles ( $\pm 15^\circ$ ).

PEM images acquired in a single detector position were initially reconstructed using a weighted backprojection algorithm similar to the used for the PEM-I system described above, or by a limited angle tomography scheme [23]. Later, the use of acquired data at two detector positions ( $\pm 15^\circ$ ) [28] to guide stereotactic biopsy motivated the use of an adapted Maximum Likelihood - Expectation Maximization algorithm.

The described acquisition scenario was compared with multiple acquisitions between the same limiting angles, at small uniform increments [29]. The results were somehow mixed, with no clear evidence of significant advantage of one acquisition scenario over the other, although less artifacts were observed with the multiple angle acquisition.

This led to a study of the complete angular sampling around the breast [30] through step and shoot acquisitions. Not surprisingly, this study showed that the complete angular sampling provided better image quality with respect to a single acquisition with stationary detectors. The study also revealed some of the weaknesses of the system, such as the low rate acquisition capability and the lack of DOI information.

Posterior work reports a new design of the scanner, now named PEM-PET [31], as it means to be a tomographic system. This system has four planar detector heads that can rotate around the breast. The detector crystal used is now LYSO, with  $2 \times 2 \times 15 \text{ mm}^3$  individual detector elements. The PEM-PET system has 2 mm FWHM resolution, possessing, as its anterior version, the ability to guide biopsy. The initial clinical studies have shown the ability of the system to detect lesions also detected by standard methods [32].

### 3.4. The Duke University — Jefferson Lab PEM system

Another system was developed at the Jefferson Laboratory and Duke University to image the compressed breast [33]. This PEM system has two opposed planar  $15 \times 20 \text{ cm}^2$  detectors that



**Figure 8.** Image of the Duke University - Jefferson Laboratory PEMsystem positioned in a mammography unit. The PEM detectors are highlighted by black arrows. From [34].

acquire data without rotational or translational movements. The detector arrays are composed of  $3 \times 3 \times 10 \text{ mm}^3$  of lutetium gadolinium oxyorthosilicate, LGSO. The scintillation light is collected by arrays of PS-PMTs. This system is used mounted on an X-ray mammography unit, although the PEM detector heads must be removed to acquire the X-ray image. The distance between the detector heads can be adjusted to match the size of the breast. Image reconstruction is performed by means of the backprojection scheme. The image spatial resolution varied from 4.8 mm to 6 mm, depending on the acceptance angles of the lines of response. An image of the system can be seen in Figure 8.

A pilot clinical trial was performed using this system [34]. This trial included 23 patients with suspected breast malignancies. Therefore, it does not provide meaningful information concerning the specificity of the technique. In this study, where the majority of the evaluated lesions had diameters smaller than 2.5 cm, PEM presented a sensitivity of 86%. The size of the three malignant lesions that PEM was unable to detect varied from 8 mm to 15 mm. The system was able to detect a 4 mm DCIS that was not detected by mammography.

### 3.5. The maxPET system

A dedicated PET camera for mammary and axillary region imaging, maxPET, was designed and constructed at the Crump Institute for Biological Imaging [35]. This group used an alternative scheme to couple the crystal arrays to the PMT's, in order to avoid the problems associated with the inactive area near the PMT edges. The maxPET system consisted of two  $15 \times 15 \text{ cm}^2$  planar scintillation detector plates, each composed of several modular detectors. The detectors are composed of arrays of  $3 \times 3 \times 20 \text{ mm}^3$  LSO crystals, each crystal array being coupled to an optical fiber which in turn is coupled to a PS-PMT. The use of the optical fiber allows the exact match between the crystal area and the active PMT dimensions, thus avoiding gaps between detector modules. It also provides better imaging close to the chest wall, since the plates are active out to the edge of the field-of-view. The main disadvantage of the fiber-optic coupling is the loss of scintillation light.

The two detector plates can be mounted in a gantry allowing variable plates separation, detector plates rotation and angular motion. Based on Monte Carlo simulation, the expected intrinsic spatial resolution of the scanner was about 2.3 mm [36]. A prototype of this system was assembled but, to our knowledge, no clinical test were ever performed.

A second prototype of this detector was build, with modified geometry and electronics. The integration of this system with a dedicated CT system was exploited [37].

### 3.6. The LBNL PEM system

The PEM scanner developed at the Lawrence Berkeley National Laboratory (LBNL) has two major differences from the PEM scanners described here: it has a rectangular geometry, with four detector plates surrounding the breast and it has Depth of Interaction measurements capabilities [38].

The system uses a 6 ns time window and has 5% sensitivity at the center of the FOV. The measured spatial resolution of the scanner is almost uniform in the entire field-of-view, ranging from 1.9 mm FWHM at the FOV centre to 2.1 mm at the FOV corner [38]. Images of a mini-Derenzo phantom show that the smallest lesion resolved by the system is 2.4 mm in diameter.

In the context of the development of this scanner, a simulation study was done to compare the presented rectangular detector configuration with a dual stationary detector system, such as some of the systems presented above. For such purpose it was used the Fisher information matrix, an analytical computation that allows to characterize how easily a change of one parameter in the source distribution can be identified from the measured data [40]. This study has shown that the rectangular system with Depth of Interaction capability has a higher signal-to-noise ratio for detection tasks and a lower bias at a given noise level for quantitation tasks. It is worth stressing that this study did not include the case of a rotating dual head scanner [39]. The LBNL PEM system consists of four detector plates that cover a rectangular  $8.2 \times 6.0 \times 5.0$  cm<sup>3</sup> field of view. The detector modules contain arrays of  $3 \times 3 \times 30$  mm<sup>3</sup> LSO crystals that are coupled to a single photomultiplier tube (PMT) in one end and to a photodiode array (PD) on the other end. The ratio between the signals of the PMT and the PD allow the estimation of the Depth of Interaction of the photon [41]. The achieved DOI resolution ranges from 6 mm FWHM at the PD end to 11 mm FWHM at the PMT end [42].

The image reconstruction task for this scanner has been subject of an intense work. In an initial stage, image reconstruction was performed with a filtered backprojection based reconstruction algorithm that took into account the existence of DOI information and the irregular angular sampling of the scanner [43, 44]. Later, a list mode penalized maximum likelihood algorithm using Gaussian priors was developed [40, 45, 46]. A Monte Carlo based scatter correction algorithm was also developed [46]. To our knowledge, this scanner has never been tested with clinical data.

### 3.7. The YAP-PEM system

The YAP-PEM prototype was developed within a collaboration of the Italian Universities of Pisa, Ferrara, Bologna and Roma [47]. The technology of this device derives from a small animal

scanner previously developed by the group. The YAP-PEM scanner has been designed with the aim of detecting 5 mm breast lesions in diameter and an activity ratio of 10:1 between the cancer and the breast tissue. The device is composed of two stationary detector heads made of yttrium aluminium perovskite (YAlO<sub>3</sub>) scintillators doped with cerium (YAP:Ce). This is a scintillator crystal that produces a light output of about 20 photons/keV, has a decay constant of 30 ns and a density of 5.4 g/cm<sup>3</sup> [48]. It has, however, a low Z number. Each detector head has a detection area of 6×6 cm<sup>2</sup> that comprises 30×30 detection elements with 2×2×30 mm<sup>3</sup> each. The system uses PS-PMTs to collect the scintillation light. The distance between the detectors can range from 5 to 10 cm, depending on the breast compression used.

For image reconstruction purposes, the ML-EM algorithm has been adapted to the planar nature of the acquired data, in order to obtain a pseudo-tomographic imaging method [49]. This method works on data that is converted into histograms that are indicated for planar data. These are known as planograms [50]. Geometrical symmetries are used to speed up the computations.

Monte Carlo simulation and image reconstruction studies performed for the YAP-PEM scanner indicate that the scanner is expected to have capability of discriminating 5 mm tumors in a target-to-background ratio of 10:1. However, due to the planar nature of the data, if two sources lie on the same axial plane, the system cannot discriminate them, as it can be seen in Figure 10.

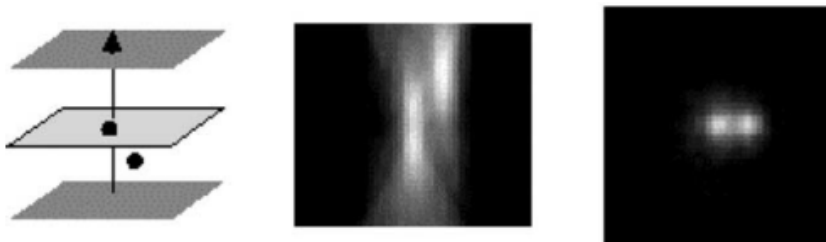


**Figure 9.** Phantom images obtained with the YAP-PEM prototype. Due to the planar nature of the scanner's data, if two sources lie on a same axial plane, the system cannot discriminate them. From [49].

### 3.8. The Clear-PEM system

The Clear-PEM system was developed within the framework of the CrystalClear collaboration, in CERN. The system, which was designed to allow the examination of the breast and the axilla regions, is composed of a dual-plate detector head that is housed in a robotic mechanical gantry, as represented in Figure 11. For the breast examination, the patient lays in the prone position with the breast hanging through an aperture in the patient. The two detector heads are positioned in each side of the breast, as represented in Figure 11, and the projection data are acquired at several angular positions. The detector heads can be positioned at different separation distances, allowing for the accommodation of different breast sizes.



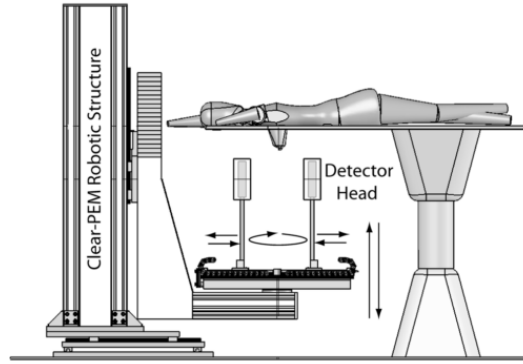


**Figure 10.** Representation of the Clear-PEM system. From [51].

The detector heads cover a  $16.2 \times 14.1 \text{ cm}^2$  FoV. Each detector head holds 96 detector modules, is constituted of a total of 3072 LYSO:Ce crystals, each crystal having  $2 \times 2 \times 20 \text{ mm}^3$ . A scheme of a detector head is shown in Figure 12a. The distribution of the crystals within the detector plates is as follows. Each detector plate is constituted of a set of four structures named supermodules, each one with  $14 \times 4 \text{ cm}^2$ , placed side by side. Each supermodule is composed of  $12 \times 2$  modules that, in turn, are composed of an array of  $4 \times 8$  LYSO:Ce crystals. Therefore, each detector plate is constituted of  $48 \times 64$  LYSO:Ce crystals.

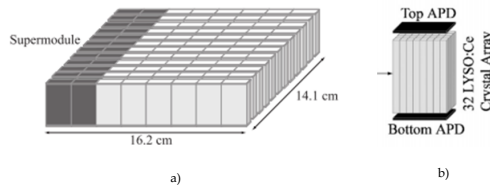


**Figure 11.** Clear-PEM detectors. a) Representation of a Clear-PEM detector head, with an highlighted detector super-module. From [51]. b) Representation of a Clear-PEM detector module with the double readout scheme. From [52].

The readout of each module is performed by two 32-pixel avalanche photodiodes that are optically coupled to each side of the module, as shown in Figure 12b. This double readout scheme allows the DOI measurement. The DOI coordinate within the crystal is estimated from the asymmetry of the collected light at the top and bottom APD pixels. Experimental results have shown that, with this scheme, it is possible to obtain a 2 mm FWHM DOI resolution [53]. This measurement is important since it increases the uniformity all over the field-of-view of the scanner. This feature is not common in the universe of the positron emission mammography dedicated scanners and therefore it is perhaps one of the most important characteristics of this scanner. The processing of the detector analogical signals, including the readout, the low noise amplification, the sampling and the storage are implemented in dedicated ASICs (Application Specific Integrated Circuits) integrated in the detection plates. The output

analogue sampled pulses are digitized by Analogue Digital Converters (ADC) and transmitted to the data acquisitions system (DAQ). This system, based on FPGA (Field Programmable Gate Arrays), is responsible for the data reduction and storage. Data is sent from here to a trigger system that selects two-photon events in coincidence within a programmable timing window and, at each trigger, the relevant data frames are sent to the acquisition PC where energy and time information are analyzed [54]. For events with more than one active crystal in a detector head, due to Compton scattering, an event reconstruction position algorithm is used to assign the coordinates of the interaction. Those events that are within the selected energy window are validated, their final coordinates being used to define the LORs that are stored in a list-mode file [53]. Images are reconstructed using 3D statistical iterative algorithms or 2D algebraic techniques [55–57]. Phantom studies showed that the scanner is suitable for millimetric tumor detection; Derenzo phantom studies showed that lesions up to 2 mm in diameter can be clearly seen; a gelatin breast phantom indicated that lesions up to 3 mm in diameter can be detected. The first prototype, installed at the Institute of Nuclear Sciences Applied to Health, Coimbra, Portugal, was used for the first tests in a preclinical environment [58].

More recently, the ClearPEM scanner has been used to create a multimodal PEM and ultrasound scanner [59]. The aim of this system is to provide high resolution, high sensitivity and high specificity metabolic information from PEM matched with 3D high resolution anatomic information. The new ClearPEM-Sonic scanner also provides elastographic information from ultrasound, further improving the specificity of the multimodality scanner. This second prototype is installed at the Hôpital Nord, in Marseille, France, and has confirmed a spatial resolution of about 1.5 mm in phantom studies. The system allows the co-registration of US/ClearPEM and elastography/ClearPEM with an alignment precision of about 2 mm. The first clinical trial has confirmed the ability to detect very small lesions only seen by MRI, although lesions very close to the chest wall are left undetected [60].

### 3.9. The MAMMI system

MAMMI (MAMmography with Molecular Imaging) is a dedicated breast PET, commercialized by Oncovision, which has certification in Europe and has recently received FDA approval [61].

Instead of the more often used small pixelated crystal arrays, this scanner uses continuous LYSO crystals coupled to PSPMTs.

The MAMMI prototype is a full ring PET consisting of 12 detector modules forming a dodecagon with a scanner aperture of 186 mm [12]. Each detector module uses 10 mm thick scintillation crystals with 40x40mm<sup>2</sup> face. The back face of the crystals are coupled to the PSPMTs. The detector has a 18% energy resolution at 511 keV, an intrinsic resolution of 1.6 mm and a DOI resolution of 4 mm.

The system aperture provides a 170 mm diameter FoV. The coincidences are allowed between a detector module and its seven opposite modules, providing a transaxial FoV aperture of 170 mm diameter. The axial FoV length is 40 mm per frame; an elevator allows the sequential move

of the ring detector in step and shoot mode to increase the axial FoV to 170 mm. A timing window of 5 ns is used.

During image reconstruction the crystal faces are discretized into  $2 \times 2 \text{ mm}^2$  pixels. Images are reconstructed with standard 3D ML-EM with a voxel size of  $1 \times 1 \times 1 \text{ mm}^3$ . The system matrix was obtained through calculation of the solid angle of every voxel with respect to the detection surface. Image reconstruction takes into account dead time, scatter and random events correction. A method for attenuation correction without a transmission scan has been developed and tested with the system [62].

Patients are imaged in the prone position, which is possible due to the existence of a breast aperture in the patient table. This allows to image regions close to the chest wall without breast compression.

The preliminary results using a 1 mm in diameter  $^{22}\text{Na}$  point like source results of 1.6 mm FWHM axial and 1.9 transaxial in the center of the FoV and less than 3 mm FWHM in most other parts of the FoV (axial) [12, 63]. The system sensitivity at the FoV center and with a wide energy window of 250-759 keV is 1 %.

A pilot study was recently conducted with 32 invasive breast cancer patients to assess the feasibility of the system for tumor detection and characterization [64]. The system sensitivity for primary tumor visualization was 97%, which equals whole body PET-CT in the same study. This included lesions close to the chest wall.

## 4. Conclusions

With two commercially available PEM scanners, there is now data from several clinical studies that confirm the high sensitivity and specificity values for PEM in different clinical situations [65, 66]. These data also allow a direct comparison with other techniques such as PET and MRI and seem to indicate that the promise of molecular imaging with dedicated instruments as a valuable adjunct technique for mammography holds true.

## Author details

Mónica Vieira Martins<sup>1,2</sup>

Address all correspondence to: mvmartins@estgp.pt

1 Polytechnic Institute of Portalegre, Portalegre, Portugal

2 Instituto de Biofísica e Engenharia Biomédica, Faculdade de Ciências, Universidade de Lisboa, Lisboa, Portugal

## References

- [1] Wahl RL. Current status of PET in breast cancer imaging, staging, and therapy. *Semin Roentgenol.* 2001 Jul;36(3):250–60.
- [2] Gopalan D, Bomanji JB, Costa DC, Ell PJ. Nuclear Medicine in Primary Breast Cancer Imaging. *Clin Radiol.* 2002 Jul;57(7):565–74.
- [3] Levin CS. Primer on molecular imaging technology. *Eur J Nucl Med Mol Imaging.* 2005 Dec;32 Suppl 2(14):S325–45.
- [4] Bayley DL, Karp JS, Surti S. Physics and Instrumentation in PET. *Positron Emission Tomography - Physics, Instrumentation and Scanners.* Springer-Verlag; 2003.
- [5] Defrise M, Kinahan PE, Christian M. Image Reconstruction Algorithms in PET. *Positron Emission Tomography - Physics, Instrumentation and Scanners.* Springer-Verlag; 2003.
- [6] Korzhik M, Fedorov A, Annenkov A, Borissevitch A, Dossovitski A, Missevitch O, et al. Development of scintillation materials for PET scanners. *Nucl Instruments Methods Phys Res Sect A Accel Spectrometers, Detect Assoc Equip.* 2007 Feb;571(1-2):122–5.
- [7] Humm JL, Rosenfeld A, Del Guerra A. From PET detectors to PET scanners. *Eur J Nucl Med Mol Imaging.* 2003 Nov;30(11):1574–97.
- [8] Bruyndonckx P, Léonard S, Liu J, Tavernier S, Szupryczynski P, Fedorov A. Study of Spatial Resolution and Depth of Interaction of APD-Based PET Detector Modules Using Light Sharing Schemes. *IEEE Trans Nucl Sci.* 2003;50(5):1415–9.
- [9] Thompson CJ, Cayouette F, Jolly D, Kecani S. A prototype modular detector design for high resolution positron emission mammography imaging. *IEEE Trans Nucl Sci.* 2003 Oct;50(5):1624–9.
- [10] Pichler BJ, Ziegler SI. Photodetectors. In: Wernick M, Aarsvold JN, editors. *Emission Tomography - the Fundamentals of PET and SPECT.* Elsevier Academic Press; 2004.
- [11] Macdonald L, Edwards J, Lewellen T, Haseley D, Rogers J, Kinahan P. Clinical Imaging Characteristics of the Positron Emission Mammography Camera: PEM Flex Solo II. *J Nucl Med.* 2009;50(10):1666–75.
- [12] Moliner L, Gonzalez AJ, Soriano A, Sanchez F, Correcher C, Orero A, et al. Design and evaluation of the MAMMI dedicated breast PET. *Med Phys Phys.* 2012;39(9):5393–6404.
- [13] Thompson CJ, Murthy K, Weinberg IN, Mako F. Feasibility study for Positron Emission Mammography. *Med Phys.* 1994;21(4):529–38.

- [14] Thompson C., Murthy K, Picard Y, Weinberg IN, Mako F. Positron Emission Mammography (PEM) - a promising technique for detecting breast cancer. *IEEE Trans Nucl Sci.* 1995;42(4):1012–7.
- [15] Bergman AM, Thompson C., Murthy K, Robar J., Clancy RL. Co-registration of positron emission mammography (pem) images and x-ray mammograms. *IEEE Nuclear Science Symposium - Conference Record.* 1997. p. 1812–6.
- [16] Robar JL, Thompson CJ, Murthy IS, Clancy R, Bergman AM. Construction and calibration of detectors for high-resolution metabolic breast cancer imaging. *Nucl Instruments Methods Phys Res - Sect A Accel Spectrometers Detect Assoc Equip.* 1997;392(1-3):402–6.
- [17] Robar J., Thompson CJ, Murthy K, Clancy RL, Bergman AM. Correction of spatial distortion, gain nonuniformity and efficiency variation in positron emission mammography. *IEEE Nuclear Science Symposium - Conference Record.* 1996. p. 1206–10.
- [18] Murthy K, Aznar M, Thompson CJ, Loutfi A, Lisbona R, Gagnon JH. Results of Preliminary Clinical Trials of the Positron Emission Mammography System PEM-I: A Dedicated Breast Imaging System Producing Glucose Metabolic Images Using FDG. *J Nucl Med.* 1994;41(11):1851–8.
- [19] Murthy K, Aznar M, Bergman AM, Thompson CJ, Robar JL, Lisbona R, et al. Positron Emission Mammographic Instrument: Initial Results. *Radiology.* 2000;215(1):280–5.
- [20] Murthy K, Jolly D, Aznar M, Thompson CJ, Sciascia P, Loutfi A, et al. Quantification in positron emission mammography (PEM) with planar detectors: contrast resolution measurements using a custom breast phantom and novel spherical hot spots. *IEEE Trans Nucl Sci.* 1999;46(6):2192–6.
- [21] Wollenweber SD, Williams RC, Beylin D, Dolinsky S, Weinberg IN. Investigation of the Quantitative Capabilities of a Positron Emission Mammography System. *IEEE Nuclear Science Symposium - Conference Record.* 2004. p. 8700–2.
- [22] Weinberg IN, Stepanov PY, Beylin D, Anashkin E, Lauckner K, Yarnall S, et al. PEM-2400 – a Biopsy-Ready PEM Scanner with Real-Time X-Ray Correlation Capability. *IEEE Nuclear Science Symposium - Conference Record.* 2003. p. 1128–30.
- [23] Weinberg I, David B, Steve Y, Anashkin E, Dolinsky S, Zavarzin V, et al. Applications of a PET Device with 1.5 mm FWHM Intrinsic Spatial Resolution to Breast Cancer Imaging. *IEEE International Symposium on Biomedical Imaging: from Macro to Nano.* 2004. p. 1396–9.
- [24] Levine EA, Freimanis RI, Perrier ND, Morton K, Lesko NM, Bergman S, et al. Positron Emission Mammography: Initial Clinical Results. *Ann Surg Oncol.* 2003 Jan; 10(1):86–91.

- [25] Tafra L, Cheng Z, Uddo J, Lobrano MB, Stein W, Berg W a, et al. Pilot clinical trial of 18F-fluorodeoxyglucose positron-emission mammography in the surgical management of breast cancer. *Am J Surg*. 2005 Oct;190(4):628–32.
- [26] Raylman RR, Majewski S, Wojcik R, Weisenberger AG, Kross B, Popov V, et al. An Apparatus for Positron Emission Mammography Guided Biopsy. *IEEE Nuclear Science Symposium - Conference Record*. 1999. p. 1323–7.
- [27] Raylman RR, Majewski S, Wojcik R, Weisenberger AG, Kross B, Popov V. Coincidence, Compton Scatter, and Object Size in Positron Emission Mammography (PEM) Imaging. *IEEE Trans Nucl Sci*. 2001;48(3):913–23.
- [28] Raylman RR, Majewski S, Weisenberger AG, Popov V, Wojcik R, Kross B, et al. Positron Emission Mammography – Guided Breast Biopsy. *J Nucl Med*. 2001;42(6):960–6.
- [29] Smith MF, Majewski S, Weisenberger AG, Kieper DA, Raylman RR, Turkington TG. Analysis of Factors Affecting Positron Emission Mammography (PEM) Image Formation. *IEEE Nuclear Science Symposium - Conference Record*. 2002. p. 2253–7.
- [30] Smith MF, Raylman RR, Majewski S, Weisenberger AG. Positron emission mammography with tomographic acquisition using dual planar detectors: initial evaluations. *Phys Med Biol*. 2004;49(11):2437–52.
- [31] Raylman RR, Virginia W, Smith MF, Kinahan PE, Majewski S. Quantification of radiotracer uptake with a dedicated breast PET imaging system. *Med Phys*. 2008;35(11):4989–97.
- [32] Raylman RR, Abraham J, Hazard H, Koren C, Filburn S, Schreiman JS, et al. Initial clinical test of a breast-PET scanner. *J Med Imaging Radiat Oncol*. 2011 Mar;55(1):58–64.
- [33] Turkington TG, Majewski S, Weisenberger AG, Popov V, Smith MF, Sampson WH, et al. A Large Field of View Positron Emission Mammography Imager. *IEEE Nuclear Science Symposium - Conference Record*. 2003. p. 1883–6.
- [34] Rosen EL, Turkington TG, Soo MS, Baker JA, Coleman RE. Radiology Detection of Primary Breast Carcinoma with a Dedicated, Large-Field-of-View FDG PET Mammography Device: Initial Experience. *Radiology*. 2005;234(2):527–34.
- [35] Doshi NK, Shao Y, Silverman RW, Cherry SR. Design and evaluation of an LSO PET detector for breast cancer imaging. *Med Phys*. 2000;27(7):1535–43.
- [36] Doshi NK, Silverman RW, Shao Y, Cherry SR. maxPET: A Dedicated Mammary and Axillary Region PET Imaging System for Breast Cancer. *IEEE Trans Nucl Sci*. 2001;48(3):811–5.
- [37] Lamare F, Bowen SL, Visvikis D, Cortes P, Wu Y, Tran V, et al. Design Simulation of a Rotating Dual-Headed PET / CT Scanner for Breast Imaging. *IEEE Nuclear Science Symposium - Conference Record*. 2005. p. 1524–9.

- [38] Wang G, Huber JS, Moses WW, Qi J, Member S, Choong W. Characterization of the LBNL PEM Camera. *IEEE Trans Nucl Sci.* 2006;53(3):1129–35.
- [39] Qi J, Kuo C, Huesman RH, Klein GJ, Moses WW, Member S, et al. Comparison of Rectangular and Dual-Planar Positron Emission Mammography Scanners. *IEEE Nuclear Science Symposium - Conference Record.* 2002. p. 1246–50.
- [40] Qi J, Klein GJ, Huesman RH, Member S. Image Properties of List-Mode Likelihood Reconstruction for a Rectangular Positron Emission Mammograph With DOI Measurements. *IEEE Trans Nucl Sci.* 2001;48(4):1343–9.
- [41] Moses WW, Derenzo SE, Melcher CL, Manente RA. Room temperature LSO pin photodiode PET detector module that measures depth of interaction. *IEEE Trans Nucl Sci.* 1995;42(4):1085–9.
- [42] Wang G, Member S, Huber JS, Moses WW, Member S, Choong W, et al. Calibration of a PEM Detector With Depth of Interaction Measurement. *IEEE Trans Nucl Sci.* 2004;51(3):775–81.
- [43] Virador PRG, Moses WW, Huesman RH, Zatsiorsky VM. Reconstruction in PET Cameras with Irregular Sampling and Depth of Interaction Capability \*. *IEEE Trans Nucl Sci.* 1998;45(3):1225–30.
- [44] Virador PRG, Moses WW, Huesman RH, Zatsiorsky VM. 3D Reconstruction in PET Cameras with Irregular Sampling and Depth of Interaction. *IEEE Trans Med Imaging.* 2001;48(4):1524.
- [45] Huesman RH, Klein GJ, Moses WW, Qi J, Reutter BW, Virador PRG. List-Mode Maximum-Likelihood Reconstruction Applied to Positron Emission Mammography (PEM) with Irregular Sampling. *IEEE Trans Med Imaging.* 2000;19(5):532–7.
- [46] Qi J, Huesman RH. Lesion Detection and Quantitation of Positron Emission Mammography. *IEEE Nuclear Science Symposium - Conference Record.* 2002. p. 2248–52.
- [47] Guerra A Del, Belcari N, Bencivelli W, Motta A, Righi S, Vaiano A, et al. Monte Carlo Study and Experimental Measurements of Breast Tumor Detectability with the YAP-PEMM prototype. *IEEE Nuclear Science Symposium - Conference Record.* 2003. p. 1887–91.
- [48] Belcari N, Camarda M, Guerra A Del, Herbert D, Motta A, Vaiano A, et al. Development of a planar head PEM system based on an array of PSPMT and YAP crystals. *IEEE Nuclear Science Symposium - Conference Record.* 2004. p. 2179–82.
- [49] Motta A, Guerra A del, Belcari N, Moehrs S, Panetta D, Righi S, et al. Fast 3D-EM reconstruction using Planograms for stationary planar positron emission mammography camera. *Comput Med imaging Graph.* 2005 Dec;29(8):587–96.



- [50] Brasse D, Kinahan PE, Clackdoyle R, Defrise M, Comtat C, Townsend DW. List-Mode Maximum-Likelihood Reconstruction Applied to Positron Emission Mammography (PEM) with Irregular Sampling. *IEEE Trans Med Imaging*. 2004;23(4):413–25.
- [51] Albuquerque E, Almeida FG, Auffray E, Barbosa J, Bastos AL, Bexiga V, et al. An overview of the Clear-PEM breast imaging scanner. 2008 IEEE Nuclear Science Symposium Conference Record. Ieee; 2008. p. 5616–8.
- [52] Amaral P, Bruyndonckx P, Carriço B, Ferreira M, Luyten J, Moura R, et al. Long-term stability of the Clear-PEM detector modules. *Nucl Instruments Methods Phys Res Sect A Accel Spectrometers, Detect Assoc Equip*. 2007 Feb;571(1-2):488–92.
- [53] Abreu MC, Aguiar JD, Almeida FG, Almeida P, Bento P, Carriço B, et al. Design and Evaluation of the Clear-PEM Scanner for Positron Emission Mammography. *IEEE Trans Nucl Sci*. 2006;53(1):71–7.
- [54] Bento P, Gonçalves F, Leong C, Lousã P, Nobre J, Rego J, et al. Performance Simulation Studies of the Clear-PEM DAQ / Trigger System. *IEEE Trans Nucl Sci*. 2006;53(4):2102–11.
- [55] Trindade A, Almeida P, Ferreira NC, Martins M V, Matela N, Oliveira N, et al. Breast Cancer Imaging Studies by Monte Carlo Simulation with Clear – PEM. *IEEE Nuclear Science Symposium - Conference Record*. 2005. p. 2103–7.
- [56] Martins M V, Matela N, Oliveira N, Trindade A, Rodrigues P, Ferreira N, et al. Clear-PEM data reconstruction using STIR. *Eur J Nucl Med Mol Imag*. 2005;32(S1):S34.
- [57] Cao L, Bugalho R, Matela N, Martins M V, Almeida P, Peter J, et al. List-Mode Maximum-Likelihood Reconstruction for the ClearPEM System. *IEEE Nuclear Science Symposium - Conference Record*. 2011. p. 4171–4.
- [58] Abrantes M, Almeida P, Botelho F, Bugalho R, Carvalho S, Ferreira CS, et al. Clear-PEM scanners: performance results and studies in preclinical environment. *IEEE Nuclear Science Symposium - Conference Record*. 2011. p. 3291–5.
- [59] Cucciati G, Auffray E, Bugalho R, Cao L, Vara N Di, Farina F, et al. Development of ClearPEM-Sonic, a multimodal mammography system for PET and Ultrasound. *J Instrum*. 2014 Mar 6;9(03):C03008–C03008.
- [60] Frisch B, Dkzf P, Bugalho R, Neves J, Silva JC, Silva R. Development of ClearPEM-Sonic - a Multimodal Positron Emission Mammograph and Ultrasound Scanner. *IEEE Nuclear Science Symposium - Conference Record*. 2011. p. 2267–72.
- [61] Fowler AM. A Molecular Approach to Breast Imaging. *J Nucl Med*. 2014;55(2):177–80.
- [62] Soriano A, González A, Orero A, Moliner L, Carles M, Sánchez F, et al. Attenuation correction without transmission scan for the MAMMI breast PET. *Nucl Instruments*

- Methods Phys Res Sect A Accel Spectrometers, Detect Assoc Equip. 2011 Aug; 648:S75–S78.
- [63] Moliner L, Benlloch JM, Carles M, Correcher C, González AJ, Orero A, et al. Performance Characteristics of the MAMMI PEMT Scanner Based on NEMA NU 2-2007. 2010 IEEE Nuclear Science Symposium Conference Record (NSS/MIC), . 2010. p. 2591–4.
- [64] Koolen BB, Aukema TS, González AJ, Vogel W V., Caballero L, Peeters MJTFDV, et al. First clinical experience with a dedicated PET for hanging breast molecular imaging. Q J Nucl Med Mol Imaging. 2013;57(1):92–100.
- [65] Berg WA, Madsen KS, Schilling K, Pisano ED, Larsen LH, Ozonoff A, et al. Breast Cancer: Comparative Effectiveness of Positron Emission Mammography and MR Imaging in Presurgical Planning. Radiology. 2011;258(1):59.
- [66] Schilling K, Narayanan D, Kalinyak JE, The J, Velasquez MV, Kahn S, et al. Positron emission mammography in breast cancer presurgical planning: comparisons with magnetic resonance imaging. Eur J Nucl Med Mol Imaging. 2011 Jan;38(1):23–36.